Dynamic Efficiency Modeling of a Marine DC Hybrid Power System

Pramod Ghimire*†, Mehdi Zadeh*, Eilif Pedersen*, and Jarle Thorstensen†
*Department of Marine Technology, Norwegian University of Science and Technology, Trondheim, Norway
†Kongsberg Digital AS, Horten, Norway
Email: pramod.ghimire@ntnu.no

***Abstract*—With the share of high-power electronic converters, the emerging marine DC hybrid power systems have been increasingly attractive for ship designers because of their higher operational flexibility. The system efficiency analysis, one of the critical factors while embracing an emerging system, requires a detailed estimation and evaluation. Conventionally, the rated efficiency for each component is the basis for the system efficiency estimation. However, the efficiency may vary with the loading conditions in any component, directly affected by the actual load and the load-sharing strategies. In this work, dynamic efficiency models are developed for the DC hybrid power system components, which are used to estimate the overall system efficiency using a realistic load power profile and a rule-based power and energy management system (PEMS). The efficiency analysis shows that the overall power efficiency increases with optimal battery usage in a hybrid power system. Moreover, three different power-sharing control strategies are compared. The modified rule-based PEMS offers the highest efficiency, while conventional diesel generator operation offers the least efficiency for the given load profile and power system configuration.**

***Index Terms*—DC Marine Hybrid Power System, Dynamic System Efficiency, Efficiency Modeling & Comparison**

I. Introduction

The marine industry is embracing the hybrid power system to reduce emissions and increase efficiency. The battery hybridization in the marine power system can be implemented in both the AC and DC power grids thanks to controllable power converters [1]. However, due to the easy inclusion of the energy storage devices (ESDs) and the variable speed operation of diesel engines, the DC power grid is considered a more feasible and efficient [2] system. The efficiency claim comes from the lower specific fuel oil consumption (SFOC) of the diesel engine for a low-load at a lower speed than the fixed speed operation [3].

In a marine power system, the combustion engines are driven by the energy content of fossil fuels. The engines' mechanical energy output goes through various stages of conversions and finally as the propulsion unit's mechanical energy output. If the auxiliary loads are not considered, the system energy efficiency can then be obtained as the ratio of energy output from the propulsion unit to the energy content in the fuel. However, in the case of the hybrid all-electric ships, the energy discharged from the battery is considered as the input energy to the power system, whereas the energy used to charge the battery is considered the load or system output. In the conventional methods, the rated efficiency of the power system components is utilized to calculate the system efficiency [4]. However, the efficiency of the components varies with their loading [5], and hence the load-sharing strategies. It is, therefore, essential to consider the actual losses in all the components to model the dynamic efficiency of a system [6].

The loss models for most of the hybrid power system components are presented in [7]. The battery loss and efficiency models are also presented in [8], [9]. The distribution of losses for the generator and propulsion drives are included in [10]. Different loss model options for the electrical machines and their efficiency modeling methodologies are presented in [11]. The efficiency evaluation through the loss models for different components involved in the wireless fast charging system is discussed in [12]. The semiconductor losses for the voltage and current source converters are presented in [13].

These loss models for each component may be incorporated in their mathematical component models. These component models are then integrated to develop the system model of a power system. The addition of loss models in the component models may increase the complexity and the computational effort. When it comes to an extensive system, it may be computationally demanding to use more accurate models for the components, and their losses [14]. Moreover, high-fidelity models usually require several parameters that may decrease flexibility to reuse such models for efficiency estimation in other power system configurations, and different types of vessels [14].

When the efficiency curves for the power system components are available, they can be used to calculate the output power from the component when the input power is known. In this work, the efficiency curves and the data for different hybrid power system components are inherited from the literature to develop the polynomial or rational polynomial equation-based efficiency models. These component models are integrated to develop a typical DC marine hybrid power system. The overall system efficiency is estimated and analyzed based on the typical operational load power profile. Moreover, the effect of load-sharing between the generator and battery in the system efficiency is also analyzed. The contribution of this work is developing a simple yet robust system efficiency model for a DC hybrid power system. The

The authors would like to thank the Research Council of Norway and Kongsberg Digital for the financial support.

developed efficiency model is computationally efficient due to eliminating the complex mathematical formulations and is reusable for various hybrid power system configurations.

This paper is organized into five sections. The system overview and the relevant component losses are explained in section II. Section III includes the component efficiency models and the system modeling methodology. The experimental validations and various simulation-based analyses for efficiency comparison are included in section IV. Section V presents the conclusion of this study.

II. System Overview

A typical marine hybrid power system with the DC power grid is implemented in this work (see Fig. 1). A generator and a battery bank supply the DC bus. The electric motor connected to each bus, acting as propulsion load, consumes the energy. The energy carriers and consumers are interfaced using the power electronic converters. The primary component capacities for the studied system are depicted in Table I.

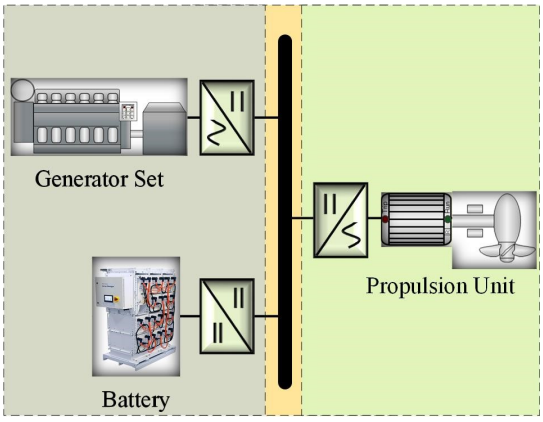

Fig. 1. Schematic of the studied system for efficiency evaluation.

TABLE I
Rated capacities.

Generation Side		Load Side	
Component	Capacity	Component	Capacity
Diesel engine	380 kW	Inverter	168 kW
Generator	360 kW	Motor	160 kW
Rectifier	378 kW		
Battery	22.5 kWh		
DC-DC Conv.	70 kW		

1) Diesel Engine: Internal combustion engines convert the chemical energy contained in the fuel to mechanical energy through combustion. During the process, there exist various losses such as combustion, exhaust, heat transfer, and mechanical (frictional) losses [15]. The specific fuel oil consumption (SFOC) curve projects the amount of fuel used to generate the required load or brake power. The engine's total input energy can be calculated based on the density and lower calorific value of the fuel. Thus, the difference between chemical energy input and mechanical energy output is the engine's actual loss. Fig. 2 depicts the SFOC curve against the load percentage for a typical fixed speed and variable speed engine. The SFOC curve comparison for the fixed and variable speed engines shows that fuel saving is achieved in a variable speed engine, especially in the lower load conditions. If the engines usually are loaded around 90% or more, then there are no significant fuel savings achieved through the variable speed engines. It shows the relevance of considering the actual loading for the SFOC or efficiency calculations. The SFOC curve for different engines varies with the size and manufacturer and is usually stated in the engine data sheet.

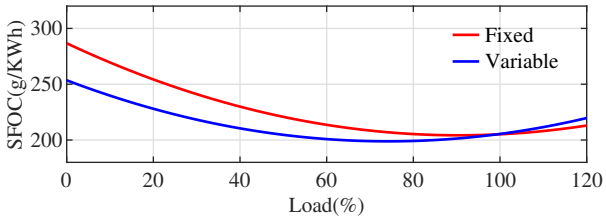

Fig. 2. Typical SFOC curves for fixed and variable speed diesel engines [6].

2) Electric Machine: In shipboard power systems, electrical machines such as synchronous generators and induction motors are widely used for electrical and mechanical power generation. As motoring and generating are reverse action, the power flow in these machines is in opposite directions. However, they consist of similar electromagnetic and mechanical components. Therefore, identical power losses occur in generators and motors. The copper, iron, and mechanical losses are the significant losses in these machines [6], [16], [17]. As the copper loss ($P_{Loss,Cu}$) is the sum of power losses in the stator and rotor windings, it is load-dependent and can be expressed as

$$P_{Loss,Cu} = I_s^2 R_s + I_r^2 R_r \tag{1}$$

where R_s and R_r are equivalent stator and rotor resistance, respectively. I_s and I_s are stator and rotor current, respectively. The iron or core loss ($P_{Loss,Fe}$) in the electric machines comprises hysteresis, eddy-current, and extra losses. It, also known as no-load losses, can be expressed as [11]

$$P_{Loss,Fe} = K_H B^2 f + K_e B^2 f^2 + K_a B^{1.5} f^{1.5} \tag{2}$$

where K_H, K_e, and K_a are hysteresis, eddy-current, and extra loss coefficients. B is peak flux density, and f is the fundamental frequency of excitation. The friction and air drag losses account for the mechanical losses ($P_{Loss,m}$), which can be expressed as a function of mechanical loss coefficient (c_m) and shaft speed (ω_m) [6].

$$P_{Loss,m} = c_m \omega_m^2 \tag{3}$$

3) Battery: The energy loss in the Li-ion battery occurs due to two different types of potential polarization, namely, ohmic and electrochemical polarization resulting in the ohmic

($E_{Loss,\Omega}$) and electrochemical ($E_{Loss,EC}$) losses [18], respectively. These losses can be calculated as

$$E_{Loss,\Omega} = \int_{SoC_0}^{SoC_t} \Delta V_\Omega \cdot C_b \cdot dSoC \tag{4}$$

$$E_{Loss,EC} = \int_{SoC_0}^{SoC_t} \Delta V_{EC} \cdot C_b \cdot dSoC \tag{5}$$

where ΔV_Ω and ΔV_{EC} are the ohmic and electrochemical polarization [18], respectively. C_b (Ah) is the nominal battery capacity and SoC (%) is battery state of charge.

4) Power Converter: The significant losses in the power converters, such as inverters, active front end (AFE) rectifiers, and DC-DC converters, comprise the conduction and switching losses. For a switch module consisting of an insulated-gate bipolar transistor (IGBT) with an anti-parallel diode, the conduction and switching losses can be expressed in generic form based on [12], [13], [19] as follows

$$P_{Loss,Cond,IGBT} = \alpha I_C (V_{CE} + r_{CE} I_C) \tag{6}$$

$$P_{Loss,Cond,Diode} = \beta I_F (V_{FW} + r_F I_F) \tag{7}$$

$$P_{Loss,Sw,IGBT} = \lambda f_{sw} (E_{on} + E_{off}) \left(\frac{I_{out}}{I_{ref}}\right) \left(\frac{V_{out}}{V_{ref}}\right)^{1.3} \tag{8}$$

$$P_{Loss,Sw,Diode} = \mu f_{sw} E_{rr} \left(\frac{I_{out}}{I_{ref}}\right)^{0.6} \left(\frac{V_{out}}{V_{ref}}\right)^{0.6} \tag{9}$$

where α and β are function of duty cycle or modulation index, V_{CE} is transistor voltage drop, and r_{CE} is on-state transistor resistance. I_F, V_{FW}, and r_F are current, voltage drop and on-state resistance of the diode, respectively. λ and μ are loss coefficients that vary with different control methods, f_{sw} is switching frequency, I_{out} is output current, and V_{out} is output voltage. I_{ref} and V_{ref} are reference values of switching loss measurement from data sheet. E_{on} and E_{off} are turn-on and turn-off energy dissipation in IGBT. E_{rr} is reverse recovery energy dissipation in anti-parallel diode.

Depending on the power converter configuration, the total loss can be estimated by summing up the losses in n switch modules. The module loss is calculated based on the conduction and switching losses in transistors and diodes.

$$P_{Loss,total} = n \cdot P_{Loss,module} \tag{10}$$

$$P_{Loss,module} = P_{Loss,IGBT} + P_{Loss,Diode} \tag{11}$$

$$P_{Loss,IGBT} = P_{Loss,Cond,IGBT} + P_{Loss,Sw,IGBT} \tag{12}$$

$$P_{Loss,Diode} = P_{Loss,Cond,Diode} + P_{Loss,Sw,Diode} \tag{13}$$

In a diode rectifier, the switching losses are negligible [7]. Unlike diode rectifiers, AFE rectifiers can either control the DC bus voltage in generator rectification or enable regenerative capability in the motor drives. AFE rectifier also improves the power factor and lowers the harmonic distortions; however, it has a slightly higher loss than diode rectifiers [20].

III. Efficiency Modeling

Typically, the efficiency of a component is stated for its nominal operating conditions including, nominal power. The required output power may not always be near its nominal power. Therefore, load-dependent efficiency data must be considered to evaluate the system efficiency for a specific operational power profile. It leads to a dynamic efficiency for both the component and the system. Thus, it is essential to analyze the lower and higher efficiency peaks during the operation such that necessary optimization algorithms can be introduced to improve the overall system efficiency. The efficiency data and the curves as a function of output power (%), extracted from the literature, are implemented.

A. Component Efficiency Modeling

The polynomial fitting for the efficiency data was first selected to make flexible and reusable efficiency models. However, the results for some components were unacceptable, even with higher degrees of the polynomial. In contrast, the rational fitting, which is the ratio of polynomials, gave promising results due to which they are implemented for some components. However, rational fitting may give a higher error for negative x-axis values. As the loading percentage in the components is either zero or greater than zero, the rational fitting drawback is a minor issue. The efficiency models for the considered components are included in Table II.

1) Engine: The engine efficiency can be expressed in terms of specific fuel oil consumption ($SFOC$) in mg/J and lower calorific heat value (h_n) in MJ/kg [15].

$$\eta = \frac{1}{SFOC \cdot h_n} \tag{14}$$

The efficiency map for a diesel engine, as a function of speed and power (see Fig. 3), is inherited from the SFOC contour plot [21].

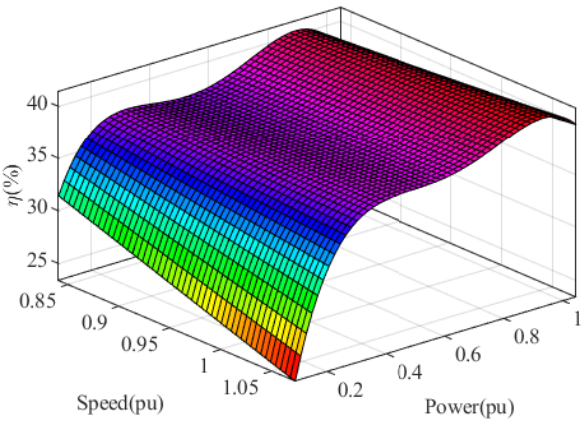

Fig. 3. Diesel engine efficiency map derived from SFOC map.

2) Electric Machine: The estimated efficiency curves for a typical synchronous generator and induction motor are depicted in Fig. 4. The efficiency curves presented in [11] are used to extract the data required for the rational polynomial fitting in both the generator and the motor.

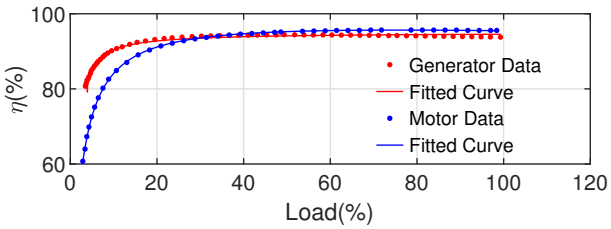

Fig. 4. Synchronous generator and induction motor efficiency curves.

3) Battery: The battery efficiency curves as a function of C-rate and SoC, based on [18], are used to fit a surface separately for the charging and discharging operation. The fitted surface plots are shown in Fig. 5. Usually, the battery is operated with a lower C-rate during the charging operation, whereas higher C-rate during the discharging operation. It results in lower polarization during charging than the discharging process. Thus, C-rate selection is associated with battery life optimization. Besides, the lower the C-rate, the higher is the battery efficiency. In contrast, the higher the SoC, the higher is the battery efficiency.

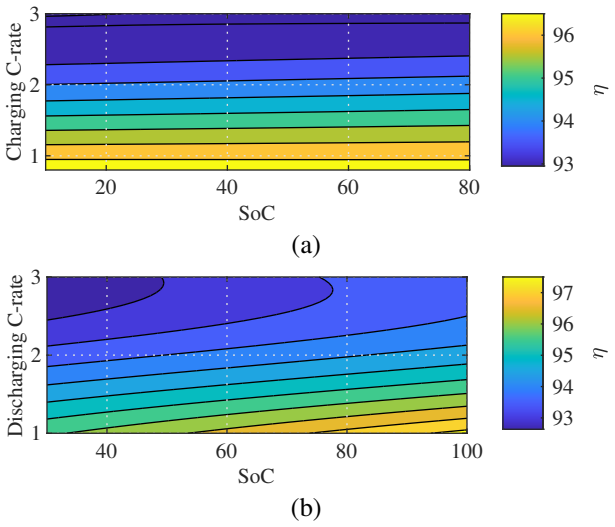

Fig. 5. The battery efficiency contour plots. (a) Charging. (b) Discharging.

4) Power Converters: The efficiency plot for the diode rectifier is shown in Fig. 6 (a), where the efficiency decreases with the increase in load percentage. A quadratic polynomial fit is used to develop the diode rectifier efficiency model based on [6]. In contrast, a rational polynomial efficiency model is developed for an AFE rectifier based on [22]. The bidirectional DC-DC converter efficiency presented in [6] is used to fit the curve. The efficiency data and the fitted curve for discharging and charging efficiency are shown in Fig. 6 (b). The typical efficiency curve of an inverter as a function of load percentage [23] is used to extract a rational polynomial-based model for its efficiency. The efficiency data and the curve fitted are shown in Fig. 6 (c).

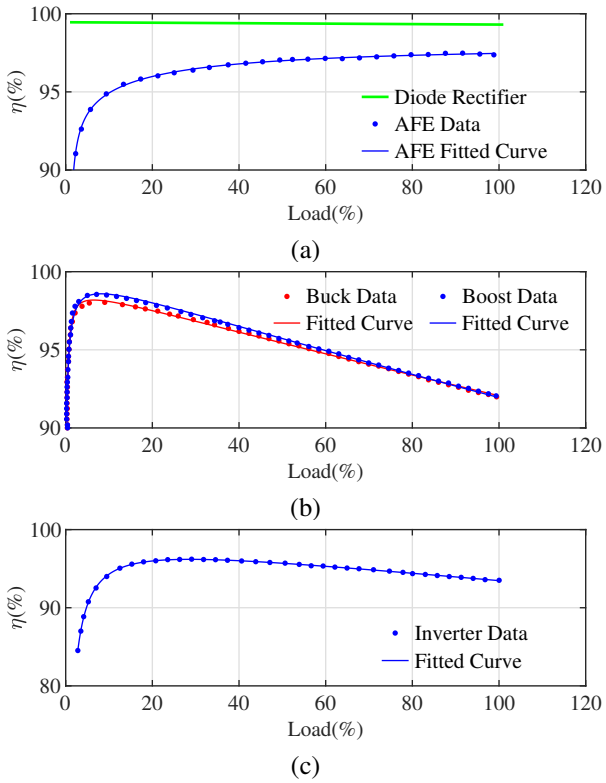

Fig. 6. Power converter efficiency curves. (a) Rectifier. (b) Bidirectional DC-DC converter. (c) Inverter.

B. System Modeling

The developed component efficiency models are integrated along with the necessary control system models such as PEMS to develop the studied hybrid power system model shown in Fig. 1. The schematic of the model integration, control system, and loss indications are presented in Fig. 7, where power and velocity are indicated by P and V, respectively. The battery in the system can be used both as a power source and power consumer, as shown by two arrows in opposite directions. The propulsion control system generates the necessary setpoint to the motor drive (inverter control system) based on the actual and required vessel speed. However, the operational profile of the propeller (P_{Load}) is known in this study. Therefore, it is assumed that the propulsion controller's setpoint to the drive is always achieved. The component efficiency models are then used to estimate the required power from other components. Both the power efficiency (η_p) and energy efficiency (η_e) are evaluated for the system as

$$\eta_p(t) = \frac{P_o(t)}{P_i(t)} = \frac{P_{Load}(t) + P_{Batt,ch}(t)}{P_{Fuel}(t) + P_{Batt,disch}(t)} \tag{15}$$

$$\eta_e(t) = \frac{\int P_o(t)dt}{\int P_i(t)dt} \tag{16}$$

where P_o and P_i are the system output and input power, respectively. $P_{Batt,ch}$ and $P_{Batt,disch}$ are battery charging and discharging power, respectively.

TABLE II
EFFICIENCY MODELS

Component	Model	R^2
Diesel Engine	$\eta = f(speed, power) = f(x,y) = 70.3504 - 57.4167x - 113.0048y + 297.4336xy - 28.9213y^2 - 466.0933xy^2 + 332.1155y^3 + 234.5816xy^3 - 228.7503y^4$	0.94
Synchronous Generator	$\eta = f(power) = f(x) = \frac{-1995.9759x^2 + 7822249.9827x + 745934.0799}{x^2 + 80634.7466x + 65138.8161}$	0.99
Induction Motor	$\eta = f(power) = f(x) = \frac{-0.03253x^2 + 100.5378x + 2.9693}{x + 1.9539}$	0.99
Battery (Charging)	$\eta = f(SoC, C-rate) = f(x,y) = 98.2006 - 0.0102x - 0.8608y + 0.0140xy - 1.3007y^2 - 0.0036xy^2 + 0.3373y^3$	0.98
Battery (Discharging)	$\eta = f(SoC, C-rate) = f(x,y) = 96.3034 + 0.0486x - 0.2323y - 0.0309xy - 1.1432y^2 + 0.0070xy^2 + 0.2499y^3$	0.98
Buck Converter	$\eta = f(power) = f(x) = \frac{114783.8353x + 45255.9937}{x^2 + 1148.0987x + 524.9216}$	0.94
Boost Converter	$\eta = f(power) = f(x) = \frac{129206.9856x^2 - 35314.5571x + 2271.6225}{x^3 + 1302.7838x^2 - 314.6492x + 13.2097}$	0.95
Inverter	$\eta = f(power) = f(x) = \frac{5.986x^2 + 156724.6199x - 1089.9521}{x^2 + 1575.4616x + 760.8591}$	0.99
Rectifier (Diode)	$\eta = f(power) = f(x) = 1.5136e^{-18}x^2 - 0.0014x + 99.456$	0.99
Rectifier (AFE)	$\eta = f(power) = f(x) = \frac{98.0557x^3 + 1237.2054x^2 - 1708.3982x + 493.2557}{x^3 + 13.2962x^2 - 17.2541x + 4.3858}$	0.99

Besides efficiency calculation, some basic system parameters such as battery SoC, engine fuel consumption, and bus voltage are required for proper system analysis. The models used in [24] are used to calculate them. The battery SoC is calculated using Ah-balance as

$$SoC = SoC_0 - \frac{1}{3600 \cdot C_b} \int_{t_o}^{t} I_b \cdot dt \tag{17}$$

where I_b is current (A), C_b is capacity (Ah), and SOC_0 is initial SoC of the battery. The fuel consumption ($\dot{m}_f$) can be calculated based on the engine output power (P_e) and specific fuel oil consumption ($SFOC$).

$$\dot{m}_f = SFOC \cdot P_e \tag{18}$$

The bus voltage is given by

$$\frac{dV_{bus}}{dt} = \frac{I_b + I_g - I_l}{C_{bus}} \tag{19}$$

where V_{bus} is bus voltage, C_{bus} is DC switchboard capacitance, I_b is battery current through the DC-DC converter, I_g is generator current through the rectifier, and I_l is load current. I_b is positive when the battery is discharging and negative when it is charging.

IV. MODEL TESTING & IMPLEMENTATION

The laboratory data from the hybrid power lab at the Norwegian University of Science and Technology (NTNU) presented in [24] is used to validate the results of this efficiency-based hybrid power system model. The propulsion load's operational power profile presented in Fig. 8 is implemented for both the experiment and the simulation.

In a DC hybrid power system, power-sharing between an ESD (battery) and a conventional engine-generator can occur following different power-sharing strategies [25], which also depends on battery SoC. For this system model's testing, power-sharing is performed using a rule-based PEMS, as presented in [26]. Few important hybrid power system parameters (generator power, battery power, and battery SoC) are validated with the experimental data. The results are depicted in Fig. 9, which show that the simulation results are well aligned with the experimental data with acceptable discrepancies. When the battery SoC is greater than the higher limit, the battery charging is reduced to inhibit overcharging issues as explained in [24]. Since the commercial control with an unknown algorithm is used in the laboratory, whereas a simplified step-based charging reduction is implemented in this work, some deviations between the experimental and simulation results can be observed after 400 s of simulation. The deviations are presented as root mean square error (RMSE) in Table III.

TABLE III
THE DEVIATION BETWEEN EXPERIMENTAL AND SIMULATED RESULTS.

Parameter	RMSE
P_{Batt} (kW)	7.57
P_{Gen} (kW)	7.60
SoC (%)	0.59

The power and energy efficiency results are depicted in Fig. 10. It shows that the power efficiency peaks are obtained when the battery is discharging. The battery charging operation increases the system load; however, it is not sufficient to move the diesel generator operational profile to the optimal region in this case. Thus, considerable efficiency improvement is not obtained during battery charging.

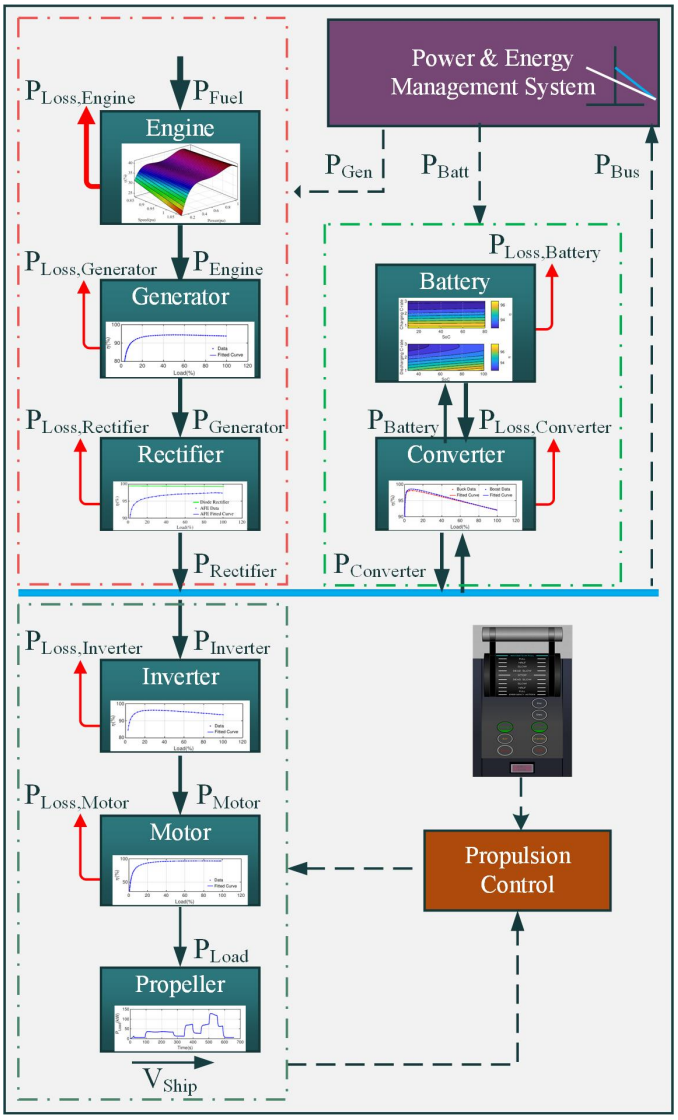

Fig. 7. Schematic of efficiency estimation methodology with loss indications.

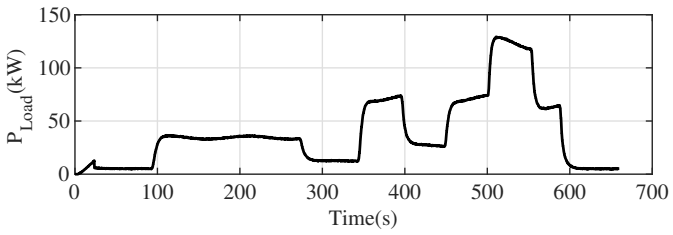

Fig. 8. The load power profile used in the lab experiment and simulations.

Various loading and power-sharing possibility can affect the overall efficiency of a hybrid power system. Three different options, namely generator-only (GO), rule-based PEMS (CL1 - Control 1), and modified rule-based PEMS (CL2 - Control 2), are compared to investigate the effects of power-sharing (control) strategies. The primary difference between CL1 and CL2 is in the power-sharing strategy between the generator and

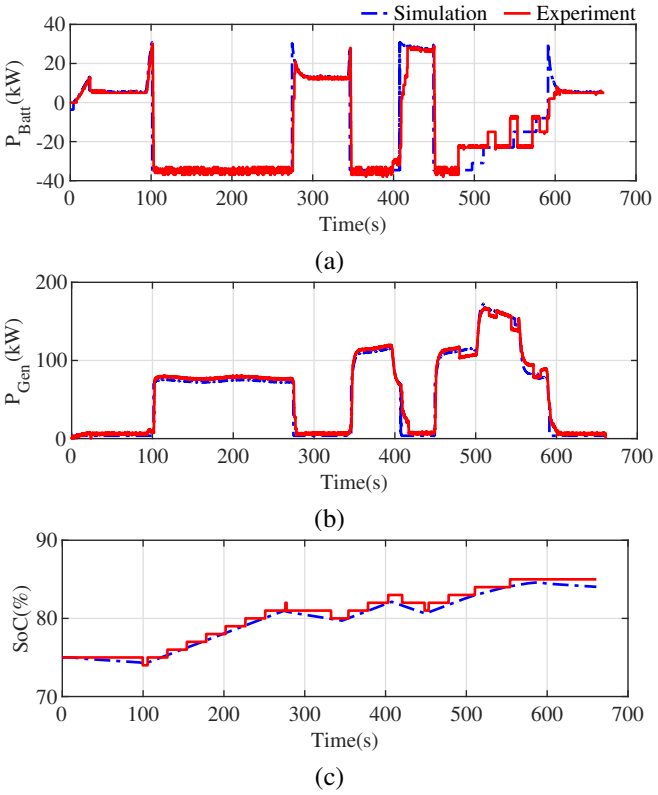

Fig. 9. Validating the simulation results with the experimental results. (a) Battery power. (b) Generator power. (c) Battery SoC.

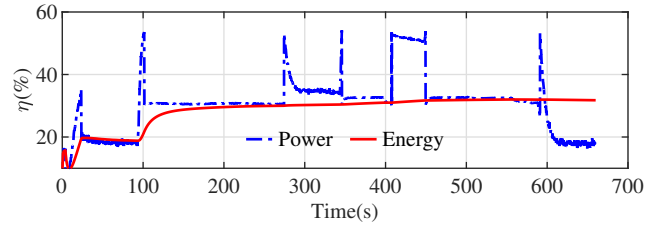

Fig. 10. System efficiency estimation for the used operational power profile.

battery. The rated maximum discharge current for the used battery in the lab is 200 A, a C-rate of approximately 3C. In CL1, the generator is active when the load is more than half of the battery's maximum discharge power. It limits the discharging C-rate to 1.5C. However, the battery is allowed to discharge until maximum discharge power (C-rate of 3C) in CL2. It enables the battery to supply higher power demand than in CL1, given the SoC of the battery is within the limit. It restricts the early activation of the diesel generator and increases battery usage. However, extensive battery use may result in faster capacity degradation. The battery efficiency decreases with an increase in C-rate. However, system efficiency may not decrease due to optimal battery use.

The load profile presented in Fig. 8 is further used to compare and analyze system efficiency. The battery is disconnected in GO, and the generator power supplies all loads. In contrast, the generator and battery share the loads following

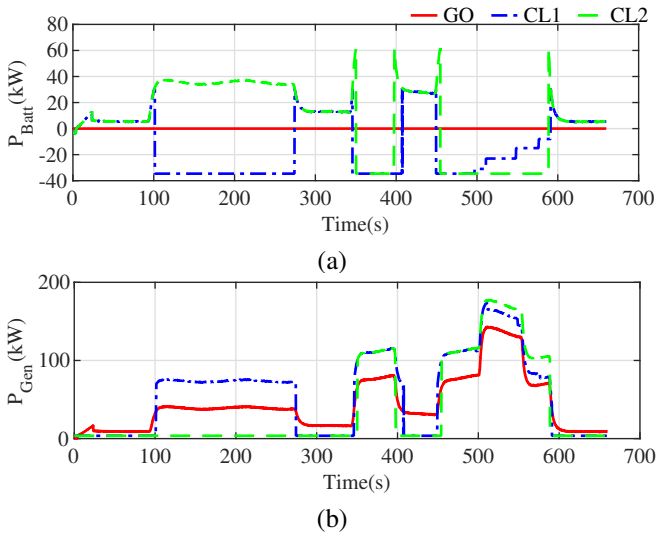

Fig. 11. Power sharing comparison for different control strategies. (a) Battery power. (b) Generator power.

a defined set of rules (see Fig. 11) in CL1 and CL2. The energy efficiency, brake-specific fuel consumption (BSFC), and battery SoC are presented in Table IV. In this case, BSFC (g/kWh) is a ratio of total fuel consumed (g) to total propulsion energy output (kWh). It is observed that CL2 stands out to be most efficient and consumes less fuel, whereas GO is least efficient. However, it consumes less fuel than CL1. It indicates that some fuel is used to charge battery in CL1, which requires investigation of stored battery energy.

TABLE IV
SPECIFIC OPERATIONAL PROFILE-BASED COMPARISON.

PEMS	η_e (%)	BSFC (g/kWh)	SoC (%)
Generator-only (GO)	27.24	204.73	-
Rule-based (CL1)	31.76	245.45	84.04
Modified rule-based (CL2)	35.82	167.99	68.75

The energy content in a battery can be reflected by the battery SoC. The battery SoC for CL1 and CL2 are depicted in Fig. 12. It is observed that the initial SoC is equal in both cases, whereas the final SoC is higher in CL1 than CL2. The SoC in CL1 is higher than the initial SoC proves that some fuel energy has been used to charge the battery in CL1. The higher the use of stored battery energy, the higher the efficiency will be. Therefore, to make a fair comparison of the efficiency between the studied PEMS, the analysis of the initial and final energy content in the battery is necessary.

The battery initial and final SoC in both control strategies needs to be equal or nearly equal for fair efficiency comparison. A fixed load of almost 50 kW is applied after 660 s to ensure that the final SoC in both cases remains at a specified level (see Fig. 13). For the extended simulation time (660 s to 900 s), a rule is defined so that the battery is charged or discharged to get near the initial battery SoC for both the control strategies (see Fig. 14).

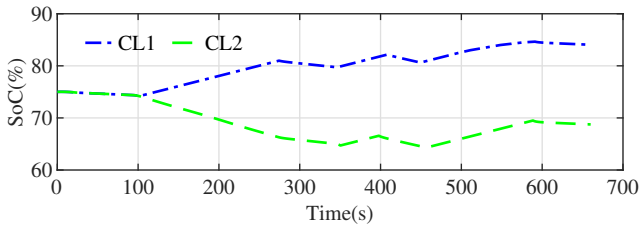

Fig. 12. SoC comparison for rule-based and modified rule-based PEMS.

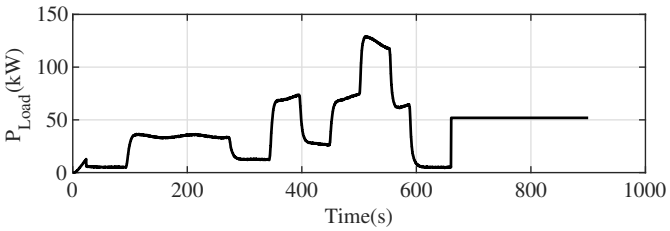

Fig. 13. The extended load power profile for efficiency comparison.

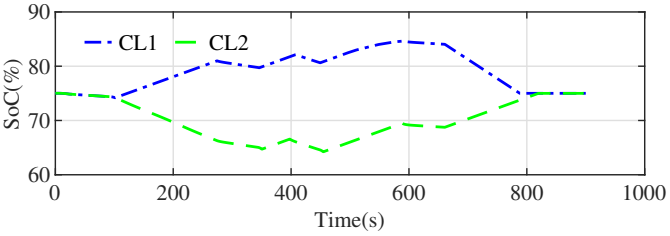

Fig. 14. SoC comparison for rule-based and modified rule-based PEMS.

As the battery in CL1 has higher SoC than the initial, it discharges while supplying the load and consuming no or significantly less fuel in the diesel generator. In contrast, as the battery in CL2 needs charging to get to the initial SoC, the diesel generator should supply power to charge the battery and supply the load. The accumulated fuel consumption in GO, CL1, and CL2 is presented in Fig. 15.

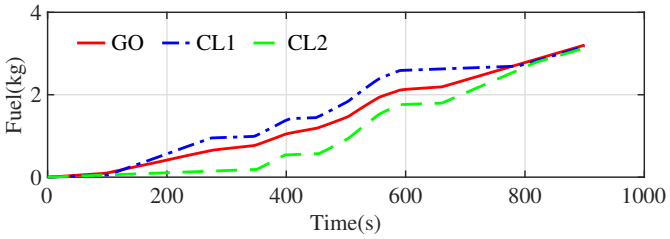

Fig. 15. Engine fuel consumption comparison for all three control strategies.

The system efficiency variation for all three control strategies is presented in Fig. 16. The battery SoC, BSFC, and system energy efficiency for the extended load profile is presented in Table V. It can be observed that the CL2 is slightly more efficient compared to CL1, whereas GO is the least efficient and consumes the highest amount of fuel.

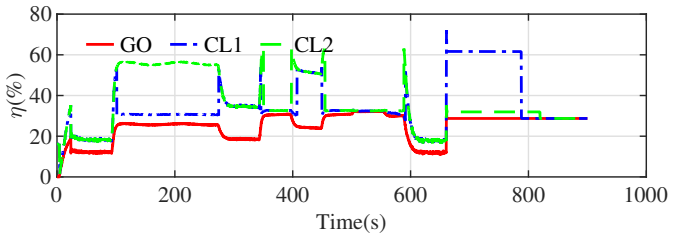

Fig. 16. System efficiency comparison using the extended load power profile.

TABLE V
EXTENDED OPERATIONAL PROFILE-BASED COMPARISON.

PEMS	η_e (%)	BSFC (g/kWh)	SoC (%)
Generator-only (GO)	27.70	274.49	-
Rule-based (CL1)	33.52	271.40	75.00
Modified rule-based (CL2)	33.97	268.31	74.99

V. CONCLUSION

A flexible and robust method for the system efficiency estimation and comparison in a marine hybrid power system is presented in this work. The dynamic component efficiency models are developed and integrated to make the studied system. It is further used to estimate the vessels' overall energy efficiency for an operational profile. The developed model is also validated using the experimental results. Besides, three different power-sharing strategies are compared. The battery SoC is maintained at the initial SoC for a fair comparison.

The simulation results showed that the power efficiency is higher when the battery is discharging. The efficiency comparison between the power-sharing strategies showed that the modified rule-based PEMS is slightly more efficient than the rule-based. The conventional generator-only operation is more than 5% inefficient along with the highest fuel consumption compared to hybrid power system configurations for the given operational profile. It shows that the vessels with a hybrid power system can be more efficient and environmentally friendly even if the battery is charged using the onboard diesel generators.

REFERENCES

[1] P. Ghimire, D. Park, M. K. M. Zadeh, J. Thorstensen, and E. Pedersen, "Shipboard Electric Power Conversion: System Architecture, Applications, Control, and Challenges [Technology Leaders]," *IEEE Electrification Magazine*, vol. 7, no. 4, pp. 6–20, Dec. 2019.

[2] M. B. Othman, N. P. Reddy, P. Ghimire, M. K. Zadeh, A. Anvari-Moghaddam, and J. M. Guerrero, "A Hybrid Power System Laboratory: Testing Electric and Hybrid Propulsion," *IEEE Electrification Magazine*, vol. 7, no. 4, pp. 89–97, Dec. 2019.

[3] E. Skjong, T. A. Johansen, M. Molinas, and A. J. Sorensen, "Approaches to Economic Energy Management in Diesel-Electric Marine Vessels," *IEEE Transactions on Transportation Electrification*, vol. 3, no. 1, pp. 22–35, Mar. 2017.

[4] A. K. Ådnanes, *Maritime electrical installations and diesel electric propulsion*, Oslo, 2003.

[5] N. Rasmussen, "Electrical Efficiency Modeling for Data Centers," American Power Conversion, Tech. Rep., 2007.

[6] B. Zahedi, L. E. Norum, and K. B. Ludvigsen, "Optimized efficiency of all-electric ships by dc hybrid power systems," *Journal of Power Sources*, vol. 255, pp. 341–354, Jun. 2014.

[7] B. Zahedi and L. E. Norum, "Efficiency analysis of shipboard dc power systems," in *IECON Proceedings (Industrial Electronics Conference)*, pp. 689–694, 2013.

[8] R. Barrera-Cardenas, O. Mo, and G. Guidi, "Optimal Sizing of Battery Energy Storage Systems for Hybrid Marine Power Systems," in *2019 IEEE Electric Ship Technologies Symposium, ESTS 2019*, pp. 293–302. Institute of Electrical and Electronics Engineers Inc., Aug. 2019.

[9] A. Gonzalez-Castellanos, D. Pozo, and A. Bischi, "Detailed Li-ion battery characterization model for economic operation," *International Journal of Electrical Power and Energy Systems*, vol. 116, p. 105561, Mar. 2020.

[10] T. I. Bø, E. Pedersen, and A. Swider, "Investigation of drivetrain losses of a DP vessel," in *2017 IEEE Electric Ship Technologies Symposium, ESTS 2017*, pp. 508–513. Institute of Electrical and Electronics Engineers Inc., Oct. 2017.

[11] T. I. Bø and E. Pedersen, "Models and Methods for Efficiency Estimation of a Marine Electric Power Grid," in *Proceedings of the ASME 2017 36th International Conference on Ocean, Offshore and Arctic Engineering OMAE2017*, Trondheim, 2017.

[12] S. Karimi, M. Zadeh, and J. A. Suul, "Evaluation of Energy Transfer Efficiency for Shore-to-Ship Fast Charging Systems," in *2020 IEEE 29th International Symposium on Industrial Electronics (ISIE)*, pp. 1271–1277. IEEE, Jun. 2020.

[13] M. H. Bierhoff and F. W. Fuchs, "Semiconductor losses in voltage source and current source IGBT converters based on analytical derivation," in *PESC Record - IEEE Annual Power Electronics Specialists Conference*, vol. 4, pp. 2836–2842, 2004.

[14] M. Sonnenberg, E. Pritchard, and D. Zhu, "Microgrid development using model-based design," in *IEEE Green Technologies Conference*, vol. 2018-April, pp. 57–60. IEEE Computer Society, Jun. 2018.

[15] J. B. Heywood, *Internal combustion engine fundamentals*, 1st ed. McGraw-Hill, Inc, 1988.

[16] C. Mademlis, J. Xypteras, and N. Margaris, "Loss minimization in wound-field cylindrical rotor synchronous motor drives," *IEEE Transactions on Power Electronics*, vol. 13, no. 2, pp. 288–296, 1998.

[17] H. Kifune, M. Zadeh, and H. Sasaki, "Efficiency Estimation of Synchronous Generators for Marine Applications and Verification with Shop Trial Data and Real Ship Operation Data," *IEEE Access*, pp. 1–1, 2020.

[18] J. Kang, F. Yan, P. Zhang, and C. Du, "Comparison of comprehensive properties of Ni-MH (nickel-metal hydride) and Li-ion (lithium-ion) batteries in terms of energy efficiency," *Energy*, vol. 70, pp. 618–625, Jun. 2014.

[19] T. Wintrich, Arendt; Nicolai, Ulrich; Tursky, Werner; Reimann, *Application Manual Power Semiconductors*. Semikron International GmbH, 2015.

[20] E. P. Wiechmann, P. Aqueveque, R. Burgos, and J. Rodriguez, "On the efficiency of voltage source and current source inverters for high-power drives," *IEEE Transactions on Industrial Electronics*, vol. 55, no. 4, pp. 1771–1782, Apr. 2008.

[21] M. R. Miyazaki, A. J. Sorensen, and B. J. Vartdal, "Reduction of Fuel Consumption on Hybrid Marine Power Plants by Strategic Loading With Energy Storage Devices," *IEEE Power and Energy Technology Systems Journal*, vol. 3, no. 4, pp. 207–217, Oct. 2016.

[22] O. Al-Naseem, R. W. Erickson, and P. Carlin, "Prediction of switching loss variations by averaged switch modeling," in *Conference Proceedings - IEEE Applied Power Electronics Conference and Exposition - APEC*, vol. 1, pp. 242–248. IEEE, 2000.

[23] N. M. Pearsall, "Introduction to photovoltaic system performance," in *The Performance of Photovoltaic (PV) Systems: Modelling, Measurement and Assessment*, pp. 1–19. Elsevier Inc., Jan. 2017.

[24] P. Ghimire, M. Zadeh, E. Pedersen, and J. Thorstensen, "Dynamic Modeling, Simulation, and Testing of a Marine DC Hybrid Power System," *IEEE Transactions on Transportation Electrification*, pp. 1–1, Sep. 2020.

[25] P. Ghimire, N. P. Reddy, M. K. Zadeh, E. Pedersen, and J. Thorstensen, "Dynamic Modeling and Real-Time Simulation of a Ship Hybrid Power System Using a Mixed-Modeling Approach," pp. 1–6. Institute of Electrical and Electronics Engineers (IEEE), Aug. 2020.

[26] L. W. Chua, T. Tjahjowidodo, G. G. Seet, and R. Chan, "Implementation of optimization-based power management for all-electric hybrid vessels," *IEEE Access*, vol. 6, pp. 74 339–74 354, 2018.